Korean J. Chem. Eng., 40(7), 1639-1649 (2023)
DOI: 10.1007/s11814-022-1344-4

pISSN: 0256-1115
eISSN: 1975-7220

Synthesis of carbon/P-zeolite composites from coal gasification fine slag and studies on adsorption characteristics for methylene blue

Rui Shu*, Jiaming Bai*, Feiqiang Guo*,†, Songbo Mao*, Qixia Qiao*, Kaiming Dong*, Lin Qian*, and Yonghui Bai,†**

*School of Low-Carbon Energy and Power Engineering, China University of Mining and Technology, 221116 Xuzhou, China
**State Key Laboratory of High-efficiency Utilization of Coal and Green Chemical Engineering, Ningxia University, Yinchuan 750021, China

(*Received 13 July 2022 • Revised 10 October 2022 • Accepted 10 November 2022*)

Abstract−Carbon/P-zeolite composites (CPZCs) were synthesized by high-temperature activation followed by hydrothermal crystallization using waste coal gasification fine slag as the raw material and NaOH as the activator. Methylene blue was selected as a dye pollutant for the adsorption experiment to investigate the adsorption property of the carbon/P-zeolite composites. It was found that the structure of CPZCs mainly depended on the mass ratio of NaOH to the coal gasification slag. At a proper NaOH to the coal gasification fine slag mass ratio of 1.0, the as-synthesized CPZC-1.0 exhibited a typical Na-P zeolite structure with a relatively high specific surface area of 200 m^2/g and pore volume of 0.21 cm^3/g. CPZC-1.0 showed excellent performance on methylene blue adsorption, with the adsorption capacity reaching 130 mg/g with removal efficiency of 81.6% at 303 K for the 100 mg/L initial methylene blue solution. The calculation results of adsorption thermodynamics indicated that the adsorption process to methylene blue by CPZCs was a spontaneous and entropy-driven endothermic process. Based on the above research, it is speculated that the adsorption mechanism of CPZCs to methylene blue might be due to the van der Waals force, intermolecular hydrogen bond and electrostatic attraction between Na-P zeolite and methylene blue.

Keywords: Coal Gasification Fine Slag, Zeolite, Methylene Blue, Adsorption

INTRODUCTION

With the rapid development of human society and economy, human production activity has produced a large number of pollutants, resulting in air, water and land pollution, which seriously threatens human health and future development [1]. In particular, industrial water pollution endangers the ecological environment and our quality of life, in which dye wastewater is considered to be one of the most serious pollution sources [2]. Methylene blue (MB), as a cationic dye, is widely used in the preparation of chemical indicators, industrial and biological dyes, and medical drugs. MB is difficult to degrade naturally due to its stable molecular structure. Thus, if dye wastewater containing MB is discharged into natural water without purification, it will cause long-term water pollution and health threat. Therefore, the effective treatment of dye wastewater is of great significance to environmental protection and sustainable development.

The current methods for dye wastewater purification mainly include biological, chemical and physical methods. Biological and chemical treatment methods mainly refer to the degradation of dyes catalyzed by organisms [3,4], molds [5] and metals [6], which is difficult to popularize on a large scale owing to the long treatment cycle and high cost. Physical adsorption methods [7], which mainly use various porous materials to realize the adsorption of pollutants in water, have the advantages of high processing rate, extensive sources for adsorbent synthesis, and recyclability, and thus have been regarded as one of the most effective technical methods for water pollution treatment [8-10]. Common adsorbents include various carbonaceous materials and porous metal and non-metal oxides such as silica gel, alumina, zeolite, and natural clay. Among these, carbonaceous materials usually exhibit excellent adsorption properties because of their large specific surface area. Also, zeolites generally have strong cation exchange value and adsorption characteristics [11], which show excellent adsorption capacity on organic matters and thus are widely used for the separation and purification of cationic organic dye wastewater.

Coal gasification technology provides a driving force for the clean utilization of coal resources. Coal gasification fine slag (CGFS) is the by-product of the coal gasification process, which has a huge annual output in China [12]. In China, more than 200 million tons of coal are used for coal gasification every year [13], resulting in tens of millions of tons of CGFS, which once reached 30 million tons in recent years [14]. However, the existing treatment schemes are basically direct landfill, which not only wastes this "resource", but also brings serious environmental pollution. The basic composition of coal gasification fine slag is residual carbon, alumina oxide, silica oxide, and a small amount of other metal oxides. Among them, alumina oxide and silica oxide are the basic raw materials for the synthesis of zeolites, and thus the coal gasification fine slag has the potential to prepare porous materials containing zeolite and porous

†To whom correspondence should be addressed.
E-mail: fqguo@cumt.edu.cn, yhbai@nxu.edu.cn

Table 1. Proximate and ultimate analysis of CGFS

Sample	Ultimate analysis (wt%)					Proximate analysis (wt%)		
	C	H	O_{diff}[a]	N	S	Ash	Volatile	Fixed carbon
CGFS	16.33	0.71	0.76	0.08	1.51	80.61	6.96	12.43

[a]Calculated by difference method

carbon structures via proper technical methods. In recent years, acid and alkali treatment methods have been investigated to improve the pore structure of CGFS to enhance its adsorption ability [15,16]. For example, Lin et al. [17] reported that H_2SO_4-treated CGFS was used as an adsorbent to remove MB dyes from aqueous solutions, and the result showed that H_2SO_4 treatment significantly improved the specific surface area and adsorption capacity of CGFS. Alkali treatment can activate the inert components in CGFS and improve its porosity [18]. Gao et al. [19] reported that NaOH activation could destroy the polymer silicate glass slag, soluble SiO_2 and polymer silicate into oligomer silicate, and the specific surface area was improved to twice the original CGFS. However, the adsorption value of CGFS is limited via simple acid and alkali treatment methods, which hinders their large-scale application.

The synthesis of zeolites using CGFS as the raw material has also been tried to obtain better structure and adsorption performance. For example, Zhao et al. [20]. prepared pure Na-X zeolite by alkali melting hydrothermal method with CGFS as the raw material and carried out MB adsorption experiments, with the maximum adsorption value reaching 127 mg/g. Furthermore, the residue carbons contained in CGFS are also considered to have adsorption performance based on their porous structure formed during the high-temperature gasification, and the synthesis of zeolite with the retention of carbon components can maximize the utilization of CGFS. Wu et al. [21] prepared a zeolite/carbon composite via the removal of impurities in CGFS, such as iron and calcium, using hydrochloric acid washing followed by mixing and stirring with NaOH solution, which showed a good adsorption performance on crystal violet in the experiment. The above research confirms that CGFS has a great potential to prepare zeolites and porous carbon structures, while the structure of synthesized zeolites is generally irregular due to the complexity of raw materials, and the synthesis process is relatively complex with the consumption of a lot of chemical reagents. Therefore, new, efficient and energy-saving preparation technologies still need to be further studied.

In this paper, a new alkali melt-hydrothermal method was developed to synthesize carbon/P-zeolite composites from CGFS. P-zeolite was successfully synthesized based on the silicon oxide and aluminum oxide in CGFS and the residue carbons in CGFS were well retained. The adsorption performance of the as-synthesized carbon/P-zeolite composites was evaluated based on the adsorption experiments of MB dye wastewater. The adsorption kinetics, isothermal, and thermodynamics were studied, based on which the adsorption mechanism of the carbon/P-zeolite composite on MB was speculated. It is hoped that this study can provide an effective way for the high-value development of coal gasification fine slag, and be applied to the treatment of polluted wastewater to realize the development concept of treating waste with waste.

Table 2. Chemical composition analysis of CGFS

Sample	Compositions (wt%)						
	SiO_2	Al_2O_3	Fe_2O_3	CaO	Na_2O	K_2O	MgO
CGFS	59.04	16.95	7.60	6.02	2.06	2.49	3.48

MATERIAL AND METHODS

1. Raw Material

The CGFS used in the experiment comes from the GSP gasification equipment of a coal gasification company in Ningxia, China. Table 1 lists the proximate and ultimate analysis results of CGFS, and Table 2 shows the XRF analysis results. After the high-temperature coal gasification, the remaining CGFS is mainly composed of ash and a certain proportion of carbon residue. It can be seen from Table 2 that the main components of CGFS are SiO_2 and Al_2O_3, which are the basic components for the synthesis of zeolites. Also, the CGFS contains some metal oxides, such as MgO, K_2O, Fe_2O_3 and CaO. Before the experiment, CGFS was ground and sieved through a 300-mesh sieve and then dried in a drying oven at 105 °C for 24 h. All the chemical reagents used in this study, such as NaOH, HCl and methylene blue, were of analytical grade.

2. Synthesis of Carbon/P-zeolite Composites

For the synthesis of carbon/P-zeolite composites (CPZCs), NaOH was used as an activator for the synthesis of zeolite and fully mixed with CGFS at a certain mass ratio. Fig. 1 displays the overall synthesis process for carbon/P-zeolite composites. The specific experimental steps are as follows: first, 1.2, 1.8, 2.4, 3.0, 3.6, 4.2 and 4.8 g of NaOH was dissolved in 50 mL deionized water, and then 3 g of CGFS was added and stirred on a heating magnetic stirrer to evaporate the water. After that, the obtained mixture was transferred to an atmosphere tubular furnace (SK-G08123K-610). The furnace was heated from room temperature to 800 °C at a rate of 10 °C/min under an N_2 flow rate of 300 mL/min and maintained at this temperature for 90 min to ensure a sufficient reaction. Then, the furnace was cooled to room temperature under the protection of N_2. The obtained materials were ground and screened with a 300-mesh sieve. Subsequently, the screened materials were mixed with deionized water at a mass ratio of 1 : 5 and transferred to a stainless steel autoclave for hydrothermal treatment at 90 °C for 18 h. The obtained materials were then washed with deionized water several times until the pH was stable, and the carbon/P-zeolite composites were finally obtained. Then, the obtained carbon/P-zeolite composites were placed in a drying oven at 105 °C for 24 h, and then ground and sieved with a 300-mesh sieve and sealed for reserve. The carbon/P-zeolite composites synthesized with different mass ratios of NaOH to CGFS were named CPZC-*x* (*x* is the mass ratio of NaOH

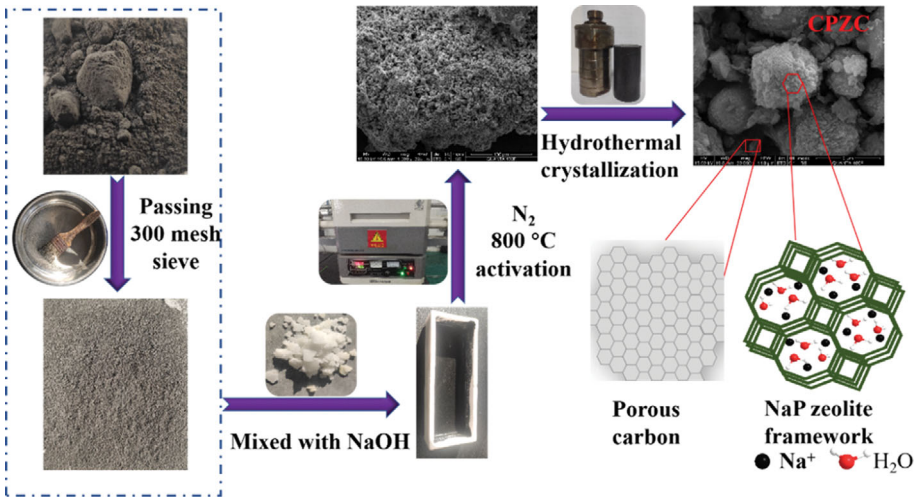

Fig. 1. Schematic illustration of the overall synthesis process for carbon/P-zeolite composites.

to CGFS).

3. Characterization Methods

The morphology of the samples was characterized by a field emission scanning electron microscopy (SEM, Quanta 400FEG, FEI) to analyze their microstructure. X-ray diffraction patterns of these samples were obtained by an X-ray diffractometer (XRD, Smart Lab (3 KW), Rigaku) in the 2θ range of 5-90° to determine their qualitative composition and structure. X-ray photoelectron spectroscopy (XPS, Thermo ESCALAB 250XI, Thermo) was used to characterize the surface chemistry of samples and determine the chemical composition and relative content. N_2 adsorption-desorption isotherms were measured at 77 K using a fast specific surface area and porosity analyzer (BET, 3Flex, Micromeritics). According to the Brunauer-Emmet-Teller equation, the specific surface area (S_{BET}) and total pore volume (V_T) of the samples were calculated based on the nitrogen adsorption value at a relative pressure of P/P^0=0.99. The specific micropore surface area (S_{mic}) and micropore volume (V_{mic}) were calculated by the t-plot method. The mesopore area (S_{mes}) and volume (V_{mes}) were obtained by the Barrett-Joyner-Halenda (BJH) method based on the adsorption branch, and the pore size distribution of the sample was calculated by the density function theory (NLDFT). A Fourier transform infrared absorption spectrometer (FT-IR, Nicolet iS50 FT-IR, Thermo) was used to analyze the surface functional groups of the samples before and after the adsorption experiment, and the spectra were recorded in the range of 4,000 to 550 cm^{-1}.

4. MB Adsorption Experiment

First, different concentrations of MB solutions were prepared. Specifically, a certain amount of dry MB was put into a certain volume of deionized water, and stirred thoroughly until completely dissolved to prepare a 200 mg/L MB solution for later use. Then, the obtained 200 mg/L MB solution was diluted with different volumes of distilled water to prepare 40-160 mg/L MB solution for adsorption experiments. In the experiment, a certain mass of CPZC-*x* was mixed with the required volume and concentration of MB solution, and the mixed solution was transferred to a 200 mL conical flask with a cap which was then oscillated in a constant temperature shaking bath (Spring SHZ-B) at 140 rpm and a preset temperature. The clear liquid was sampled by a needle filter at a specified time, which was then detected at the 665 nm wavelength of an ultraviolet spectrophotometer (Mapada, UV-1800) to determine its concentration; the adsorption value at the corresponding time was calculated. In the experiment, the adsorption value (q_t) at time t is obtained according to Eq. (1), and the removal efficiency of MB (η_t) is calculated based on Eq. (2).

$$q_t = \frac{(C_0 - C_t)}{w} \times V \quad (1)$$

$$\eta_t = \frac{(C_0 - C_t)}{C_0} \times 100\% \quad (2)$$

where, C_0 (mg/L) and C_t (mg/L) are concentrations of MB solution at the initial time and time t; V (L) is the volume of MB solution; w (g) represents the mass of CPZC-*x*.

RESULTS AND DISCUSSION

1. Characterization of CPZC Samples

The XRD patterns of CGFS and the CPZCs were obtained to further confirm their crystal compositions, as displayed in Fig. 2. The main crystals of CGFS were quartz (SiO_2) and mullite ($3Al_2O_3 \cdot 2SiO_2$). However, the diffraction peaks of quartz and mullite disappeared in CPZC-*x* samples and new crystal diffraction peaks appeared. CPZC-0.4 exhibited obvious diffraction peaks at 21, 23.1, 27.3, 29.7, 31.0, 34.8 and 38.5°, corresponding to the existence of nepheline (JCPDS, No. 76-1858). This was due to the lower mass ratio of NaOH to CGFS resulting in insufficient activation of inert components and insufficient alkalinity of the hydrothermal crystallization reaction system. The synthesized CPZC-1.0 exhibited significant diffraction peaks at 12.4, 17.6, 21.6, 28.1 and 33.8°, which corresponded to the formation of Na-P zeolite (JCPDS, No. 80-0699) [22]. By further improving the alkalinity of the hydrothermal system, the XRD pattern of CPZC-1.6 exihibited very similar diffraction peaks of Na-P zeolite to that of CPZC-1.0, while the

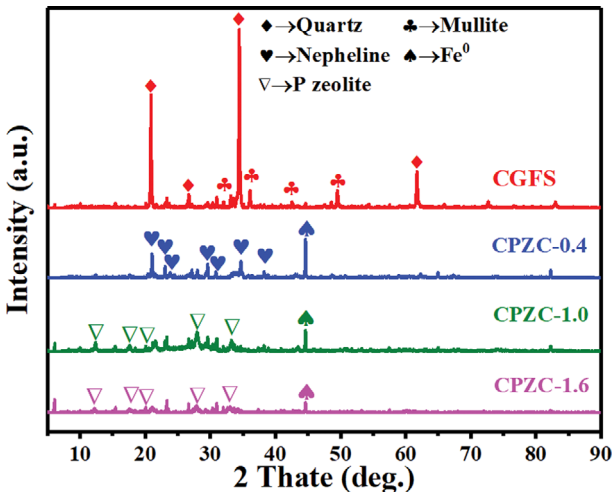

Fig. 2. XRD patterns of the CGFS, CPZC-0.4, CPZC-1.0 and CPZC-1.6.

intensity of the peaks at each position was obviously weakened, indicating that high alkalinity was not suitable for the crystallization of Na-P zeolite in the hydrothermal system, and part of the crystal phase was transformed into other amorphous substances. At the same time, obvious diffraction peaks of Fe^0 (JCPDS, No. 87-0721) were detected at 44.6° in all these three samples, indicating that the carbon in CGFS had a reduction reaction with Fe_2O_3. It has been reported that NaOH can also act as an activator for the preparation of activated carbons via chemical etching [23], and therefore the residue carbon in CGFS may also be activated during the activation process. Thus, CPZC-1.0 may have a porous structure containing both the Na-P zeolite and porous carbon structures.

Fig. 3 illustrates the SEM images of CGFS and three typical CPZC samples of CPZC-0.4, CPZC-1.0 and CPZC-1.6. As shown in Fig. 3(a), the raw CGFS contains a large number of SiO_2 microspheres and some amorphous metal oxides. During the synthesis of CPZCs, the SiO_2 microspheres undergoes destruction and recrystallization, resulting in significant changes in their morphology. The microstructure of CPZC-0.4 presents an irregular thick plate and columnar shape, as shown in Fig. 3(b), which is the nepheline structure generated under the low mass ratio of NaOH to CGFS. From Fig. 3(c), the shape and structure of CPZC-1.0 become regular, showing a unified polyhedral crystal shape. The crystals grow on the outer surface of large particles and belong to Na-P zeolite. Compared with CPZC-1.0, CPZC-1.6 exhibits a similar shape, as illustrated in Fig. 3(d), while the structural characteristics of zeolite in CPZC-1.6 become weaker and some zeolite crystals are converted into other substances.

The XPS spectrum of CPZC-1.0 is shown in Fig. 4(a) to investigate its surface elemental composition. The peaks at around 75 and 103 eV are attributed to the existence of Al2p and Si2p [24], and the peaks at 530 and 1,072 eV correspond to O1s and Na1s. Thus, it can be concluded that the four elements constituting Na-P zeo-

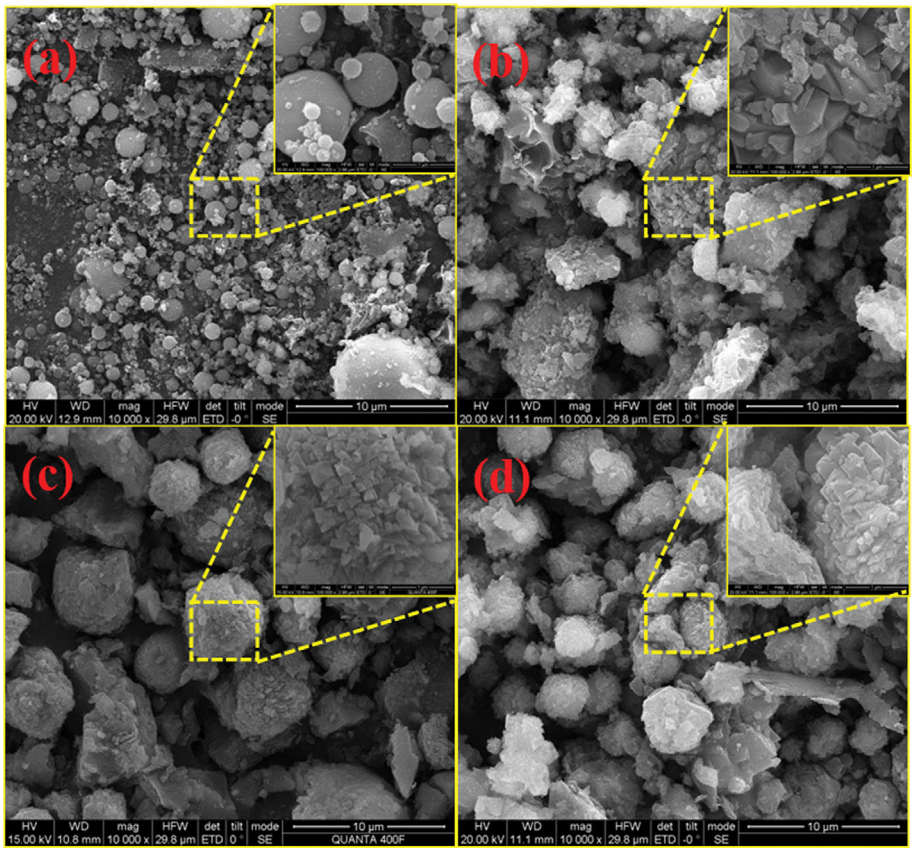

Fig. 3. SEM images of (a) CGFS, (b) CPZC-0.4, (c) CPZC-1.0 and (d) SEM images of CPZC-1.6.

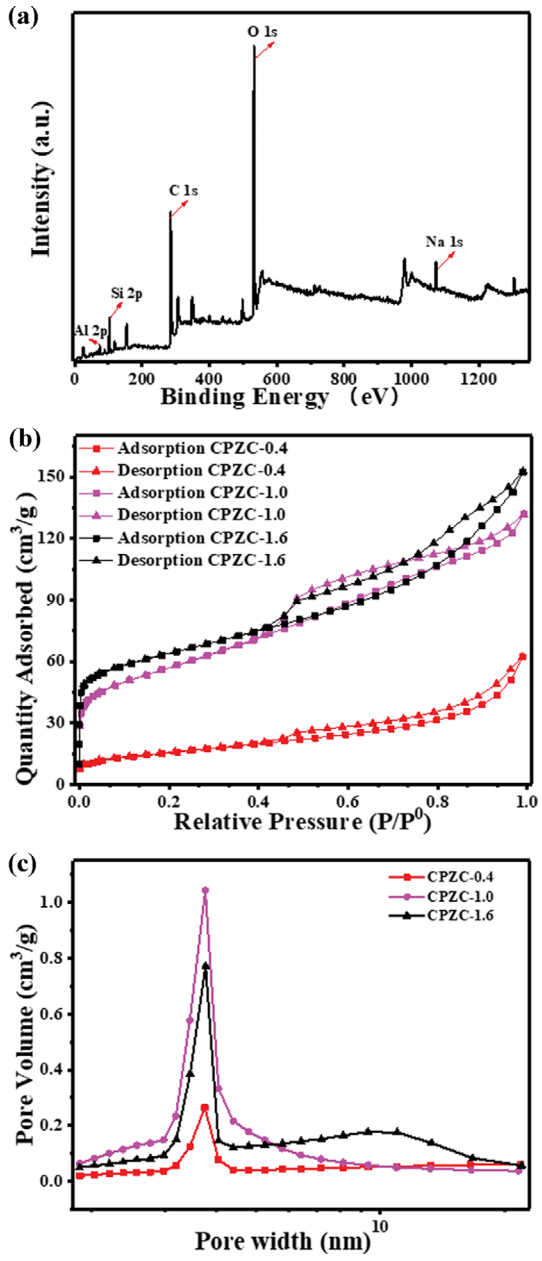

Fig. 4. (a) XPS spectrum of CPZC-1.0. (b) N_2 adsorption-desorption isotherms and (c) pore size distributions of CPZC-0.4, CPZC-1.0 and CPZC-1.6.

lite are well reflected in the corresponding positions of the XPS spectrum [25]. At the same time, a high-intensity peak corresponding to C1s appears at around 285 eV, which further confirms that the carbon in CGFS is retained in CPZC-1.0.

The N_2 adsorption-desorption isotherms of CPZC-0.4, CPZC-1.0 and CPZC-1.6 are depicted in Fig. 4(b). The N_2 adsorption capacity of CPZC-1.0 and CPZC-1.6 increase sharply at a very low relative pressure region, which indicates that there are many micropores in the structure. However, much weaker low-pressure adsorption is observed for CPZC-0.4, indicating that CPZC-0.4 possesses fewere microporous structures. It can be inferred that NaOH only participated in the reaction with SiO_2 and Al_2O_3 when NaOH was insufficient, and the residual carbon was not activated into porous carbon. However, when sufficient NaOH was provided, NaOH participated not only in the reaction with SiO_2 and Al_2O_3 but also in activation of residual carbon, and therefore porous carbon could be formed containing a large number of micropores. The adsorption-desorption isotherms of the three samples do not overlap, but hysteresis loops were formed related to the presence of mesoporous structures. According to the classification of IUPAC, the hysteresis loops of the three materials (P/P^0 range between 0.46 and 0.99) correspond to type IV with H3 hysteresis loops. The micropore filling at low relative pressure and capillary condensation of P/P^0 at about 0.4 indicates a similar micro-mesoporous structure between CPZC-1.0 and CPZC-1.6. In addition, the typical H3 hysteresis loops of CPZC-1.0 and CPZC-1.6 did not reach equilibrium when the relative pressure approached the saturated steam pressure, demonstrating that the material contained slit-shaped pores, which is a typical feature of the zeolite pore structure [26]. The difference in the hysteresis loop between CPZC-1.0 and CPZC-1.6 may be due to the inconsistency of crystal type and crystallinity. Fig. 4(c) illustrates the pore size distribution of the three samples, showing that the pore structure of the three samples is mainly mesoporous. CPZC-0.4 mainly contains mesopores, which is generally attributed to nepheline crystallization. Due to the low crystallinity and underdeveloped pores of nepheline, the S_{BET} of CPZC-0.4 was only 55 m^2/g, as shown in Table 3. Both CPZC-1.0 and CPZC-1.6 possess the Na-P zeolite structure [27,28], and thus they have a large number of mesopores at around 3.7 nm [29]. In comparison, CPZC-1.0 with higher crystallization purity of Na-P zeolite exhibits more centralized pore size distribution, and the S_{BET} reached 200 m^2/g and the V_T reached 0.20 cm^3/g. For CPZC-1.6, part of the crystal form is transformed into mesoporous amorphous materials with larger pore size, and thus there is a certain number of pores at 5-17 nm. However, the specific surface area of CPZC-1.6 is even higher than that of CPZC-1.0 due to the sufficient activation, and its S_{BET} and V_T reach 210 m^2/g and 0.24 cm^3/g, respectively.

2. Effect of the Mass Ratio of NaOH to CGFS on Adsorption

The adsorption performance of CPZC-*x* synthesized under different mass ratios of NaOH to CGFS for dye wastewater was explored using MB as a model pollutant. The dynamic adsorption process was recorded, and the results show that the adsorption pro-

Table 3. Porosity parameters of the CPZC samples

Sample	S_{BET} (m^2/g)	S_{mic} (m^2/g)	S_{mes} (m^2/g)	V_T (cm^3/g)	V_{mic} (cm^3/g)	V_{mes} (cm^3/g)	D_{av} (nm)
CPZC-0.4	55	6.0	49.0	0.10	0.01	0.09	6.98
CPZC-1.0	200	36.0	164	0.20	0.02	0.18	4.07
CPZC-1.6	210	86.0	124	0.24	0.04	0.20	4.50

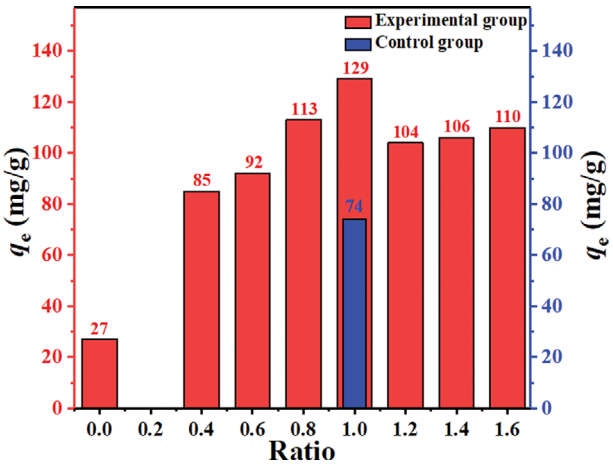

Fig. 5. Adsorption capacity of CPZC-*x* with different mass ratios of NaOH to CGFS and P-1.0.

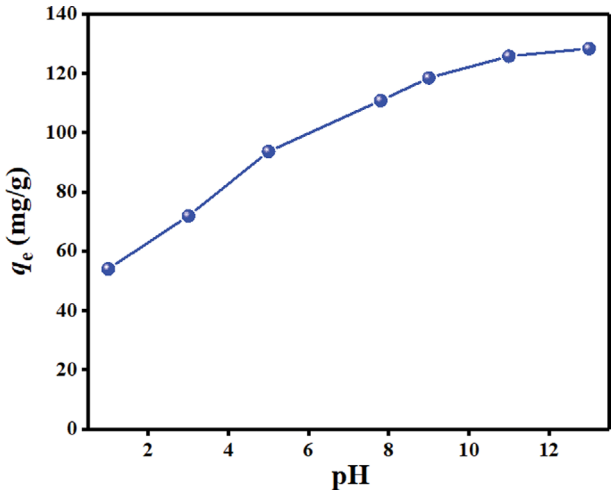

Fig. 6. Relationship between adsorption capacity of CPZC-1.0 and initial pH of MB solution.

cess had two stages with different adsorption rates, including the rapid adsorption stage at the beginning and the subsequent slow stage. The adsorption equilibrium was generally reached at about 900 min in all experiments. The adsorption value at 1,440 min was selected as a reference to compare the maximum adsorption value of CPZC-*x* samples under the same conditions. Seven groups of CPZC-*x* (0.05 g) with mass ratios of 0.4, 0.6, 0.8, 1.0, 1.2, 1.4 and 1.6 were used as adsorbents in the experimental groups, and the raw CGFS (the mass ratio of NaOH to CGFS was 0) was also used as control group. 80 mL of MB solution (100 mg/L) was used as the adsorbent in each test, and the experiment was carried out in a constant temperature shaking bath at 298 K and 140 rpm. The experimental results are shown in Fig. 5. The adsorption values of CPZC-*x* were significantly improved when the mass ratio increased from 0.4 to 1.0, and values were significantly higher than that of CGFS. Under high-temperature conditions, the inert components such as quartz and mullite in CGFS were activated by NaOH [30]. Nepheline crystals were formed by hydrothermal crystallization at the mass ratio of 0.4, and the adsorption capacity was significantly improved in comparison with that of CGFS. By further increasing the amount of NaOH, Na-P zeolite began to form, which significantly improved the adsorption performance of CPZCs. The maximum adsorption capacity of 129 mg/g was achieved by CPZC-1.0. However, further increase of NaOH mass ratio leads to the excessive alkalinity of the hydrothermal system, which may inhibit the formation of Na-P zeolite. Therefore, the adsorption capacity significantly decreases if the NaOH mass ratio is over 1.0 due to the reduction of Na-P zeolite structures in the CPZCs. As a consequence, 1.0 was considered to be the appropriate mass ratio of NaOH to CGFS for the synthesis of Na-P zeolite in this work. In addition, Na-P zeolite without carbon (P-1.0) was prepared as the control group of CPZC-1.0 by activation (the mass ratio of NaOH to CGFS is 1.0) in an air atmosphere followed by the same hydrothermal method. By comparing the adsorption capacity of CPZC-1.0 and P-1.0, it can be found that the adsorption capacity of P-1.0 is 74 mg/L, which is much lower than that of CPZC-1.0. It is speculated that the adsorption performance of porous carbon in CPZC-1.0 may be even higher than that of Na-P zeolite with the same quality. CPZC-1.0 was selected as the best adsorbent for subsequent adsorption experiments.

3. Effect of Initial pH on Adsorption

It is reported that the pH of a solution is an important factor affecting the adsorption capacity. In this work, the effect of the initial pH of MB solution on the adsorption value of CPZC-1.0 was studied in the pH range of 1.0-13.0 to explore the adaptability of CPZC-1.0 adsorption capacity to pH. In the experiments, 80 mL of MB solution with a concentration of 100 mg/L was selected, and the amount of CPZC-1.0 was 0.05 g. The experimental temperature was controlled at 298 K and the adsorption time was 1,440 min. The experimental results are shown in Fig. 6. At a low pH range, Si-OH and Al-OH groups on the surface of the zeolite were protonated into $Si\text{-}OH^{2+}$ and $Al\text{-}OH^{2+}$, while MB was an alkaline dye and its chromogenic group was positively charged [31]. Therefore, the MB molecules were electrostatically repulsed with the protonated surface groups of CPZC-1.0, resulting in a decrease in the adsorption capacity. With the gradual increase of pH, Si-OH and Al-OH groups were deprotonated into $Si\text{-}O^-$ and $Al\text{-}O^-$, which increased the density of negatively charged adsorption sites on the zeolite surface. Thus, the combination of the MB and CPZC-1.0 surface groups was promoted with the increase of pH value to improve the adsorption capacity.

4. Isothermal Adsorption Experiment

To further analyze the relationship between the equilibrium concentration and equilibrium adsorption capacity of CPZC-1.0 to MB solution, isothermal adsorption experiments were carried out at 293, 303 and 313 K. 80 mL MB solution was used in each experiment at the concentrations of 40, 60, 80, 100, 120, 140 and 160 mg/L. 0.05 g of CPZC-1.0 was used in each experiment; the experimental results are recorded in Fig. 7. Ce and q_e represent the concentration and adsorption capacity when the adsorption reached equilibrium, respectively. The number of MB molecules increased with the increase of soulution concentration, and the adsorption capacity increased rapidly at low concentrations based on the sufficient adsorption sites. By further increasing the concentration of MB solution, the increase of the adsorption capacity slowed and

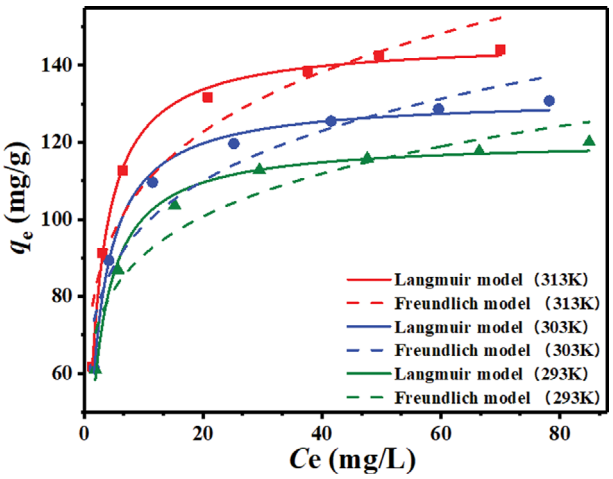

Fig. 7. Isothermal adsorption and Langmuir and Freundlich fitting models.

Table 4. Isothermal parameters for adsorption of MB onto CPZC-1.0

Isotherms	Parameters	Temperatures		
		298 K	298 K	298 K
Langmuir	q_m (mg/g)	121	132	146
	K_L (L/mg)	0.496	0.504	0.527
	R_L	0.0198	0.0195	0.0186
	R^2	0.989	0.993	0.997
Freundlich	K_F (mg/g(L/mg)$^{1/n}$)	64.1	67.7	73.3
	n	6.63	6.20	5.81
	R^2	0.903	0.898	0.891

tended to be flat, which was affected by the relatively limited adsorption sites at high concentrations. The removal efficiency was calculated according to Eq. (2). The removal efficiency of MB in the adsorption process decreased with the increase of concentration, which may be due to the decrease in the ratio of adsorption sites to MB molecules, causing competitive adsorption on the surface of CPZC-1.0 [32].

The Langmuir and Freundlich isothermal adsorption models were used for fitting analysis [33]. Fig. 7 compares these two isothermal adsorption fitting models and the obtained isothermal adsorption parameters are listed in Table 4. The q_m represents the theoretical monolayer saturated adsorption capacity, K_L is the Langmuir equilibrium constant, R_L is the dimensionless constant, K_F is the Freundlich constant, n is the Freundlich constant, and R^2 is the correlation coefficient. The R^2 of the Langmuir model is higher than that of the Freundlich model, indicating that Langmuir isothermal adsorption model is more suitable for describing the adsorption of MB by CPZC-1.0. The Langmuir model is based on the monolayer coverage of adsorbate molecules on the uniform surface of adsorbent with energy equivalent adsorption position, indicating that the adsorption of MB on CPZC-1.0 should be uniform monolayer adsorption. Also, the calculated value of R_L is between 0 and 1, which indicates that the Langmuir isotherm is an ideal adsorption type according to the Langmuir model theory. Although the fitting degree of the Freundlich model is lower than that of the Langmuir model, it can also be used as a reference since its R^2 reaches 0.9. The Freundlich index n is more than 1, suggesting that CPZC-1.0 is favorable to the adsorption process of MB in the Freundlich model theory. In addition, the isothermal adsorption test results show that the adsorption efficiency and adsorption capacity increased with the increase of temperature, which may be due to the higher temperature promoting the intermolecular movement and speeding up the contact and adsorption between adsorbate and adsorbent. The temperature effect was further analyzed by subsequent adsorption thermodynamic calculation.

Table 5. Thermodynamic parameters for adsorption of MB onto CPZC-1.0

T (K)	ΔG^o (KJ/mol)	ΔH^o (KJ/mol)	ΔS^o (KJ/mol·K)
293 K	−6.89		
303 K	−7.61	5.84	0.41
313 K	−8.59		

5. Adsorption Thermodynamics

The occurrence degree and driving factors of CPZC-1.0 adsorbing MB were studied by calculating three important parameters of adsorption thermodynamics, including standard Gibbs free energy (ΔG^o, kJ/mol), standard adsorption enthalpy (ΔH^o, kJ/mol), and standard adsorption entropy (ΔS^o, kJ/mol·K). The three parameters were calculated based on Eq. (3) and Eq. (4).

$$\Delta G^o = -RT\ln K^o \tag{3}$$

$$\ln K^o = -\frac{\Delta H^o}{RT} + \frac{\Delta S^o}{R} \tag{4}$$

where, R (8.314 J/mol·K) represents the general gas constant, K^o is the adsorption thermodynamic equilibrium constant, and T (K) is the absolute temperature of thermodynamics.

Table 5 lists the three thermodynamic calculation results. The spontaneous adsorption of MB by CPZC-1.0 was further confirmed by the negative values of ΔG^o [34]. With the increase of temperature, the value of ΔG^o decreases, indicating that heating is a favorable driving factor for the adsorption process [35], which is also consistent with the results obtained in the isothermal adsorption experiments, that is, the equilibrium adsorption capacity increases with the increase of temperature. The positive value of ΔH verifies that the adsorption behavior is endothermic [36], and the positive promotion of temperature on the adsorption is further confirmed [37]. The positive value of ΔS^o reflects that interaction between MB and the adsorption sites of CPZC-1.0 enhances the randomness of the solid-liquid interface and the degree of chaos. Also, the positive ΔS^o of the system indicates that the adsorption process tends to be stable and is an entropy-driven.

6. Adsorption Kinetics

An adsorption kinetics experiment was carried out to explore the influencing factors of adsorption equilibrium time and adsorption rate. 80 mL of MB solutions with initial concentrations of 100 and 40 mg/L were used, and 0.05 g of CPZC-1.0 was used. The experimental temperature was controlled at 303 K, and the adsorption values at different moments were recorded within 1,440 min.

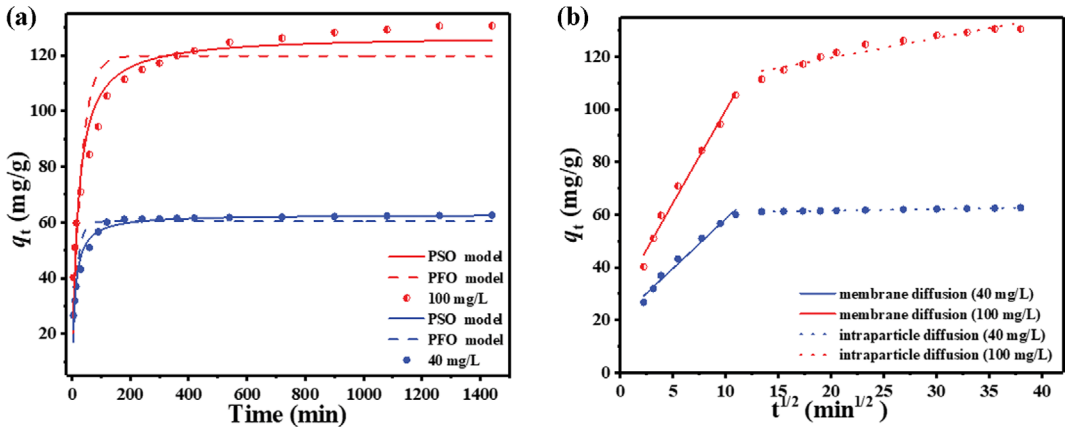

Fig. 8. Adsorption kinetics: (a) PFO and PSO fitting model; (b) ID fitting model.

The results are displayed in Fig. 8(a), showing that the adsorption process can be divided into two stages. At the initial stage, the adsorption capacity of CPZC-1.0 to MB increases rapidly, and the adsorption of 100 and 40 mg/L MB solutions begins to enter the second stage at 180 and 60 min, respectively. The second stage is the slow adsorption stage, the increase of adsorption capacity slows and reaches adsorption saturation at 900 and 120 min, respectively. The final adsorption capacity of 40 mg/L MB solution was 63 mg/g with the removal efficiency of 98.9%, while the final adsorption capacity of 100 mg/L MB solution was 130 mg/g with the removal efficiency of 81.6%.

The rate-limiting steps of the adsorption process were analyzed by the pseudo-first-order (PFO), pseudo-second-order (PSO), and intraparticle diffusion (ID) model [38], as shown in Fig. 8(b). Table 6 summarizes the fitting kinetic parameters. The PFO and PSO kinetic fitting models are shown in Fig. 8(a). $q_{e,exp}$ is the adsorption capacity recorded in the experiment, $q_{e,cal}$ is the adsorption capacity calculated by the model, k represents the adsorption rate constant, K_{id} is the diffusion rate constant. The value of the influence degree of the boundary layer on the adsorption rate is represented by c, and R^2 is the correlation coefficient. It can be seen that the R^2 fitted by the PSO kinetic model is higher than that of the PFO kinetic model, and $q_{e,cal}$ of the PSO model is also closer to $q_{e,exp}$. Thus, the PSO model is more suitable for describing the adsorption process of MB by CPZC-1.0. The PSO kinetic model is a hypothetical model controlled by the chemical adsorption mechanism in the adsorption process. The highly consistent PSO kinetic model with the adsorption process reveals that the adsorption rate-limiting step is mainly influenced by the chemisorption mechanism. More specifically, it is mainly influenced by the number of adsorption sites on CPZC-1.0, which involves electron sharing or electron transfer between MB and the adsorption sites [34,39]. In addition, according to Weber and Morris's ID model theory, the particle diffusion process in the adsorption process can be divided into two stages, including the process of adsorbate diffusion to the outer surface of the adsorbent (membrane diffusion), and the process of adsorbate transfer from the outer surface to the inner surface through the pores of the adsorbent (intra particle diffusion). According to the result of the ID kinetic fitting model in Fig. 8(b), the adsorption process is fitted as two straight lines without passing through the origin, proving that the adsorption process includes membrane diffusion and intraparticle diffusion. The first linear part is the membrane diffusion of MB molecules from the liquid phase to the surface of CPZC-1.0, and the large slope corresponds to a fast membrane diffusion rate. The second linear part is the process of MB molecules entering CPZC-1.0 channels from the surface. When MB molecules on the surface of CPZC-1.0 diffuse into the channels and gradually accumulate, the increase of diffusion resistance slows the adsorption, and the adsorption process gradually reaches the equilibrium state. At the same time, by comparing the adsorption process of MB solution with the initial concentration of 100 and 40 mg/L, it was found that the K_{id} of MB solution with higher concentration was faster, which was attributed to the increase in the proportion of adsorbate and adsorbent by the higher concentration of MB solution, thus enhancing the mass transfer process.

Table 6. Kinetic parameters of PFO, PSO and ID model fitting

Kinetics	Parameters	CPZC-1.0	
		100 mg/L	40 mg/L
PFO	$q_{e,exp}$ (mg/g)	130	62.6
	$q_{e,cal}$ (mg/g)	120	60.4
	k_1 (1/min)	0.0335	0.0653
	R^2	0.828	0.871
PSO	$q_{e,cal}$ (mg/g)	127	62.8
	k_2 (1/min)	0.000390	0.00160
	R^2	0.95313	0.97261
ID	$K_{id,1}$ (mg/g min$^{1/2}$)	7.06	3.77
	c_1 (mg/g)	28.9	20.7
	R_1^2	0.983	0.982
	$K_{id,2}$ (mg/g min$^{1/2}$)	0.753	0.0613
	c_2 (mg/g)	104	60.3
	R_2^2	0.924	0.999

7. Adsorption Mechanism

The large specific surface area and pore volume of CPZC-1.0 show that it has an excellent pore structure, which is conducive to

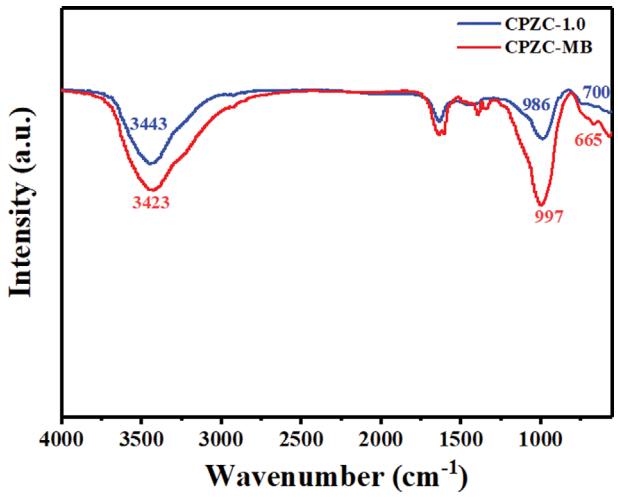

Fig. 9. FTIR comparison of CPZC-1.0 before and after adsorption.

the contact between adsorbate and adsorbent and provides sufficient adsorption sites. The pore structures of CPZC-1.0 mainly come from the Na-P zeolite and porous carbon structures in CPZC-1.0. The porous carbon structures mainly play a part in physical adsorption. As the main adsorbent, Na-P zeolite provides chemical adsorption to MB, and chemical adsorption is generally accompanied by the change of functional groups. Therefore, the fresh CPZC-1.0 and spent CPZC-1.0 separated after the adsorption experiment (CPZC-MB) are characterized by FT-IR, as shown in Fig. 9, and the mechanism of chemical adsorption was investigated by comparing their functional groups. The obvious changes in functional groups mainly occurred at 3,400, 1,000 and 700 cm^{-1}. The absorption peaks of the two samples near 3,400 cm^{-1} are attributed to the O-H group of Si-OH.

Since the O-H groups on CPZC-1.0 easily lose H^+ in the solution and become negatively charged groups, which absorb positively charged MB^+ by electrostatic attraction, leading to the wider and stronger O-H adsorption peak in FI-IR. The possible adsorption mechanism is shown in Fig. 10. Also, the adsorption performance of CPZC-1.0 as a function of pH indicates the hypothesis of electrostatic adsorption. Another possible adsorption mechanism is that the O-H groups on CPZC-1.0 produce hydrogen bonding with the N atom of the MB molecule, thus shifting its tensile vibration frequency to the direction of low wavenumber, as shown in Fig. 10. Electrostatic attraction and hydrogen bond generation are also consistent with the electron pair sharing and transfer mentioned in the chemical adsorption mechanism mentioned in the previous kinetic analysis. The fingerprint region of the infrared spectrum is between 400 and 1,300 cm^{-1}, which changes with a slight change in the molecular structure. The peak at around 1,000 cm^{-1} corresponds to the vibration of Si-O-Si in the Na-P zeolite structure. The molecular structure of CPZC-1.0 changes after the adsorption of MB, resulting in the deviation of the peak strength and location. Similarly, the movement and enhancement of the Si-OH bond absorption peak near 700 cm^{-1} are also due to the change of molecular structure after adsorption.

CONCLUSIONS

A new method for the synthesis of carbon/P-zeolite composites from coal gasification fine slag was designed via NaOH activation and subsequent hydrothermal crystallization. The structure of the as-synthesized composites was significantly influenced by the mass ratio of NaOH to CGFS. A nepheline structure was generated under the low mass ratio range of NaOH to CGFS, while part of the zeolite was transformed into an amorphous substance with a larger pore size at an excessively larger mass ratio range. CPZC-1.0 with the NaOH to CGFS ratio of 1.0 exhibits an excellent Na-P zeolite structure with the best adsorption performance in this work. The specific surface area of CPZC-1.0 reached 200 m^2/g with the pore size distribution mainly at around 3.5 nm. For the 100 mg/L MB solution, the adsorption capacity of CPZC-1.0 reached 130 mg/g

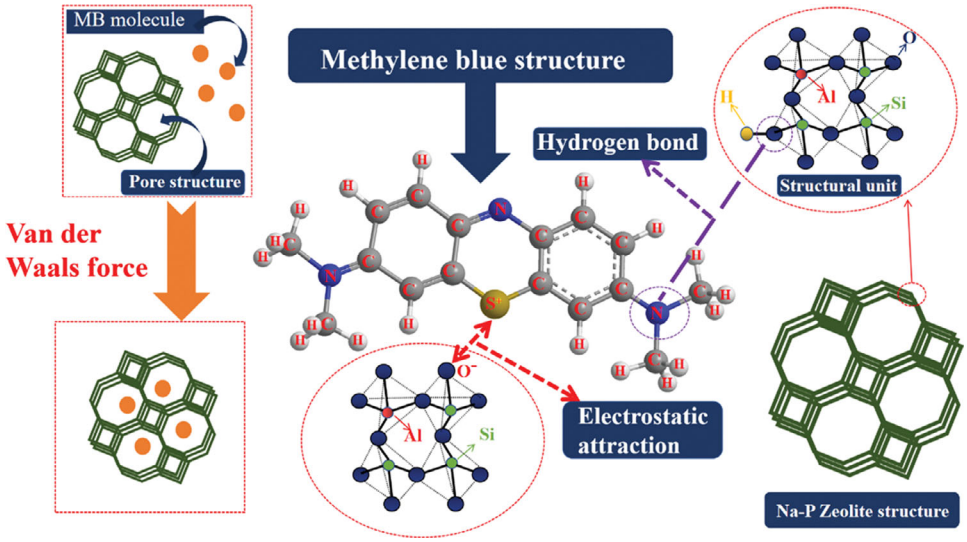

Fig. 10. The adsorption mechanism of MB adsorbed by CPZC-1.0: van der Waals force, electrostatic attraction and intermolecular hydrogen bond.

with the removal efficiency of 81.6% at 303 K. The best fitting of the PSO and Langmuir model indicated that the adsorption process was mainly controlled by the chemical adsorption mechanism. The fitting results of the ID model proved that the adsorption process included membrane diffusion and intraparticle diffusion, and the adsorption rate was mainly limited by the membrane diffusion rate. Through thermodynamic analysis, it was confirmed that adsorption was an entropy-driven spontaneous process, in which the increase of temperature was conducive to the adsorption. Electrostatic attraction and hydrogen bond generation are supposed to be the main mechanism for the adsorption of methylene blue.

AUTHOR CONTRIBUTIONS

Rui Shu: Formal analysis, Data curation, Software, Investigation, Writing – original draft. Jiaming Bai: Data curation, Software, Writing – review & editing. Feiqiang Guo: Methodology, Conceptualization, Resources, Writing – review & editing, Supervision. Songbo Mao: Resources, Writing – review & editing. Qixia Qiao: Writing – review & editing. Kaiming Dong: Writing – review & editing. Lin Qian: Writing – review & editing. Yonghui Bai: Writing – review & editing.

FUNDING

This work is supported by the project of the key research plan of Ningxia (2021BEE03011) and Foundation of State Key Laboratory of High-efficiency Utilization of Coal and Green Chemical Engineering (Grant No. 2022-K23).

DATA AVAILABILITY

The data generated during the present study are available from the corresponding authors on reasonable request.

DECLARATIONS

Conflict of interest The authors declare that they have no conflict of interest.

Novelty Statement

The concept of treating waste with waste is of great significance to the sustainable development of human society. A feasible and scalable strategy for the synthesis of carbon/P-zeolite composites (CPZCs) was designed in the work using the waste coal gasification fine slag as the precursor and NaOH as an activator. At a NaOH to the coal gasification slag mass ratio of 1 : 1, a typical Na-P zeolite and porous carbon composite (CPZC-1.0) was successfully synthesized with a relatively high surface area. The great potential of CPZC-1.0 in the purification of dye wastewater was confirmed through methylene blue adsorption. The adsorption capacity of CPZC-1.0 reached 130 mg/g, with a high removal efficiency of 81.6% at 303 K for a 100 mg/L initial methylene blue solution. This work provides a new example for the conversion and treatment of industrial inorganic solid wastes such as coal gasification fine slag to prepare high-value functional materials.

REFERENCES

1. Z. Zhou, J. Liu, N. Zhou, T. Zhang and H. Zeng, *J. Environ. Manage.*, **295**, 113048 (2021).
2. Y. Huang, B. Zhou, R. Han, X. Lu, S. Li and N. Li, *Environ. Sci. Pollut. Res. Int.*, **27**, 7188 (2020).
3. M. F. Imron, S. B. Kurniawan, A. Soegianto and F. E. Wahyudianto, *Heliyon*, **5**, e02206 (2019).
4. G. Bal and A. Thakur, *Mater. Today: Proc.*, **50**, 1575 (2022).
5. A. Yadav, P. Yadav, A. K. Singh, V. Kumar, V. C. Sonawane, Markandeya, R. N. Bharagava and A. Raj, *Bioresour. Technol.*, **340**, 125591 (2021).
6. G. Elango and S. M. Roopan, *J. Photochem. Photobiol. B*, **155**, 34 (2016).
7. M. Rafatullah, O. Sulaiman, R. Hashim and A. Ahmad, *J. Hazard. Mater.*, **177**, 70 (2010).
8. Y. Zhao, S. A. Qamar, M. Qamar, M. Bilal and H. M. N. Iqbal, *J. Environ. Manage.*, **300**, 113762 (2021).
9. W. Zhang and Z. Zhou, *Nanomaterials*, **7**, 16 (2017).
10. N. U. M. Nizam, M. M. Hanafiah, E. Mahmoudi, A. A. Halim and A. W. Mohammad, *Sci. Rep.*, **11**, 8623 (2021).
11. Y. Zhang, J. Dong, F. Guo, Z. Shao and J. Wu, *Minerals*, **8**(3), 116 (2018).
12. M. Ahmaruzzaman, *Prog. Energy Combust. Sci.*, **36**, 327 (2010).
13. M. Du, J. Huang, Z. Liu, X. Zhou, S. Guo, Z. Wang and Y. Fang, *Feul*, **224**, 178 (2018).
14. X. Liu, Z. Jin, Y. Jing, P. Fan, Z. Qi, W. Bao, J. Wang, X. Yan, P. Lv and L. Dong, *Chin. J. Chem. Eng.*, **35**, 92 (2021).
15. S. Wang, Y. Boyjoo and A. Choueib, *Chemosphere*, **60**, 1401 (2005).
16. J. Zhang, J. Zuo, Y. Jiang, D. Zhu, J. Zhang and C. Wei, *Solid State Sci.*, **100**, 106084 (2020).
17. J. X. Lin, S. L. Zhan, M. H. Fang, X. Q. Qian and H. Yang, *J. Environ. Manage.*, **87**, 193 (2008).
18. N. T. Dinh, L. N. H. Vo, N. T. T. Tran, T. D. Phan and D. B. Nguyen, *RSC Adv.*, **11**, 20292 (2021).
19. X. Gao, Y. Dai, Y. Zhang, X. Zhai and F. Fu, *Clay Clay Miner*, **64**, 695 (2016).
20. Y. P. Zhao, D. X. Guo, S. F. Li, J. P. Cao and X. Y. Wei, *Desalin. Water Treat.*, **185**, 355 (2020).
21. Y. H. Wu, K. Xue, Q. L. Ma, T. Ma, Y. L. Ma, Y. G. Sun and W. X. Ji, *Micropor. Mesopor. Mater.*, **312**, 110742 (2021).
22. M. R. Abukhadra, S. M. Ali, E. A. Nasr, H. A. A. Mahmoud and E. M. Awwad, *ACS Omega*, **5**, 14656 (2020).
23. R. L. Tseng, *J. Colloid Interface Sci.*, **303**, 494 (2006).
24. M. Maharana and S. Sen, *Waste Biomass Valori.*, **13**, 1695 (2021).
25. Y. Cheng, L. Xu, Z. Jiang, C. Liu, Q. Zhang, Y. Zou, Y. Chen, J. Li and X. Liu, *Chem. Eng. J.*, **417**, 128090 (2021).
26. M. D. Torres and J. Seijo, *Ind. Crop. Prod.*, **86**, 273 (2016).
27. Y. Zhang, H. Han, X. Wang, M. Zhang, Y. Chen, C. Zhai, H. Song, J. Deng, J. Sun and C. Zhang, *J. Hazard. Mater.*, **415**, 125627 (2021).
28. S. Bohra, D. Kundu and M. K. Naskar, *Mater. Lett.*, **106**, 182 (2013).
29. J. M. Lucero, J. M. Crawford, C. A. Wolden and M. A. Carreon, *Micropor. Mesopor. Mater.*, **324**, 111288 (2021).
30. V. Volli and M. K. Purkait, *J. Hazard. Mater.*, **297**, 101 (2015).
31. S. Wang, M. Soudi, L. Li and Z. H. Zhu, *J. Hazard. Mater.*, **133**, 243 (2006).

32. S. Lu, Q. Liu, R. Han, J. Shi, M. Guo, C. Song, N. Ji, X. Lu and D. Ma, *Chem. Eng. J.*, **409**, 128194 (2021).
33. N. Belachew and H. Hinsene, *Silicon*, **14**, 1629 (2021).
34. X. Zhang, J. Gao, S. Zhao, Y. Lei, Y. Yuan, C. He, C. Gao and L. Deng, *Environ. Sci. Pollut. Res. Int.*, **26**, 32928 (2019).
35. F. Guo, X. Li, X. Jiang, X. Zhao, C. Guo and Z. Rao, *Colloids Surf., A*, **555**, 43 (2018).
36. E. Alver and A. Ü. Metin, *Chem. Eng. J.*, **200-202**, 59 (2012).
37. L. Krishna, K. Soontarapa, N. K. Asmel, M. A. Kabir, A. Yuzir, W. Z. Yaacob and Y. Sarala, *Desalin. Water Treat.*, **150**, 348 (2019).
38. F. Salimi, M. Eskandari and C. Karami, *Desalin. Water Treat.*, **85**, 206 (2017).
39. J. Yan, Y. Li, H. Li, Y. Zhou, H. Xiao, B. Li and X. Ma, *Microchem. J.*, **145**, 287 (2019).